Supporting Information

Schumann *et al.* 10.1073/pnas.0803634105

SI Text

FMR and Rock Magnetic Properties. Two traits of FMR spectra are generally indicative of magnetofossils: sharpness of peaks and asymmetry (1). Peak sharpness (reflected in the empirical α parameter) is due to biological control and should be similar for bacterial magnetite and the novel forms. Asymmetry is controlled in large part by the effective anisotropy field, B_{an}. Proper calculation of B_{an} for a chain of magnetite particles should be done by using a chain-of-spheres model *à la* Moskowitz *et al.* (2), a calculation that has not yet been done. For a uniaxial single-domain particle, $B_{an} = \mu_0 M_s \Delta N$, where μ_0 is the magnetic permeability of free space, M_s is saturation magnetization, and ΔN, the difference by long-axis parallel and long-axis perpendicular demagnetization factors, is a function of the width/length ratio. For the fields at which resonance occurs, the particles in a chain are expected to rotate in parallel; thus, we can approximate B_{an} of a chain by $f \mu_0 M_s \Delta N$, where ΔN is calculated as though the chain is a single particle and 1-f is the fraction of this "particle" that constitutes empty space and therefore has a zero saturation magnetization. A single uniaxial particle with a width/length ratio of 0.12 (B_{an} of ≈250 mT) is therefore essentially indistinguishable under FMR from a chain of approximately eight touching equidimensional particles, or a chain of ≈18 ≈40-nm equidimensional particles with an ≈5-nm interparticle spacing. By volume, the average bacterial magnetofossil observed by Kopp *et al.* (3) had a width/length ratio of 0.6 and a length of ≈185 nm. One such particle, when isolated, would have B_{an} of 94 mT. A chain of five such particles touching, or ≈11 such particles with ≈20-cm interparticle spacing, would generate a B_{an} of ≈250 mT. Unfortunately, the novel magnetofossils do not appear to have a distinctive magnetic fingerprint recognizable in bulk rock magnetic properties, as can be seen by consideration of their expected FMR and rock magnetic properties.

Coercivity analysis is a potentially more fruitful approach. Moskowitz *et al.* (2) present data indicating that magnetite chains remagnetize not through parallel rotation but through fanning. A chain of particles therefore demagnetizes at lower field strengths than would a single particle of the same size, although at higher fields than isolated particles [as demonstrated directly through the mutant studies of Kopp *et al.* (4)]. FORC analysis of the PETM clay at Ancora shows a small fraction of particles with room-temperature coercivities of ≈120–140 mT, consistent with magnetite particles with width/length ratios of less than ≈0.14 and volumes greater than ≈0.002 μm^3 [i.e., lengths greater than ≈470 nm; values are calculated following Diaz-Ricci and Kirschvink (5)]. In isolation, the average coercivity of the observed bacterial particles should be ≈44 mT, and the largest and most elongate bacterial particles [length of ≈450 nm, width-to-length ratio of 0.20, as plotted in figure 5 of Kopp *et al.* (1)], should have a coercivity of ≈108 mT. However, this coercivity would be enhanced by chain alignment, so even the high coercivity tail of the FORC diagram cannot unambiguously be interpreted as the product of the observed unusually large biogenic magnetite.

Paleontology Searching for Modern Analogues. We searched the *Treatise on Invertebrate Paleontology* (B, Protista 1, Charophyta (6); C, Protista 2 volumes 1 and 2, Sarcodina, chiefly "Thecamoebians" and Foraminiferida (7); D, Protista 3, Protozoa, chiefly Radiolaria, Tintinnina (8); E, Archaeocyatha, Porifera (9); E revised volume 1, Archaeocyatha (10); E revised, volume 2, Porifera (11); E revised volume 3, Porifera (12); F, Coelenterata (13); F supplement 1, Coelenterata, Rugosa and Tabulata (14)) for modern or ancient morphological analogues to the presumed eukaryote "armored" by spearhead-like magnetite particles shown in Fig. S1 and Movie S1.

Although numerous species control or induce calcium carbonate mineralization in radial "spikes" (either as parts of a skeletal framework or, dissimilar to the PETM magnetofossils, as globules containing inner microvasculatures) in *Protista* (specifically within *Rotaliina*, *Calcarinidae*, *Hantkeninidae*, *Astrolonchidae*, *Staurosphaeridae*, *Pentasphaeridae-Cubosphaeridae*, *Astrosphaeridae*, *Phacodiscidae-Coccodiscidae*, *Parathuramminidae*, *Euchitoniilae*, *Theocorythidae*, *Castanellidae*, *Chapmaninae*, and *Pegidiinae*), there are no organisms whose radial outgrowths share the doubly anisotropic (convex "stalk" and concave "head") shape and the range of within-organism size and shape variation exhibited by the "Magnetic Death Star" eukaryote imaged in Fig. S1 and Movie S1.

Porifera spicules can grow to macroscopic scales. Some sponges (especially among *Choiidae*, *Plakinidae*, and *Pachastrellidae*) produce complex or sharp spicules, sometimes composed of multiple, radiating, or reticulated elements; and originally calcareous or siliceous spicules may be pseudomorphed or else coated by iron oxide (especially goethite, as in ref. 6). All sponge spicules, however, are templated by an internal protein framework interwoven with layers of biomineral crystallites, clearly distinct from the wholly inorganic, single-crystal morphology of the novel biomagnetites described here from the New Jersey PETM magnetofossil *Lagerstätte*.

1. Kopp RE, *et al.* (2006) Chains, clumps, and strings: Magnetofossil taphonomy with ferromagnetic resonance spectroscopy. *Earth Planet Sci Lett* 247:10–25.
2. Moskowitz BM, *et al.* (1988) Magnetic properties of magnetotactic bacteria. *J Magn Magn Mater* 73:273–288.
3. Kopp RE, *et al.* (2007) Magnetofossil spike during the Paleocene–Eocene thermal maximum: Ferromagnetic resonance, rock magnetic, and electron microscopy evidence from Ancora, New Jersey, United States. *Paleoceanography* 22:PA4103, doi: 10.1029/2007PA001473.
4. Kopp RE, *et al.* (2006) Ferromagnetic resonance spectroscopy for assessment of magnetic anisotropy and magnetostatic interactions: A case study of mutant magnetotactic bacteria. *J Geophys Res Solid Earth* 111:B12S25, doi: 10.1029/2006JB004529.
5. Ricci JCD, Kirschvink JL (1992) Magnetic domain state and coercivity predictions for biogenic greigite (FE3S4)—A comparison of theory with magnetosome observations. *J Geophys Res Solid Earth* 97:17309–17315.
6. Feist M, *et al. Treatise on Invertebrate Paleontology, Part B, Protoctista 1 (Charophyta)*, ed Kaesler RL (The Geological Society of America & The University of Kansas, Boulder & Lawrence), pp 1–170.
7. Loeblich AR, Tappan H (1964) *Treatise on Invertebrate Paleontology, Part C, Protista 2 (Sarcodina, Chiefly "Thecamoebians" and Foraminiferida)*, ed Moore RC (The Geological Society of America & The University of Kansas, Boulder & Lawrence), pp 1–900.
8. Shackleton Campbell A, Moore RC (1954) *Treatise on Invertebrate Paleontology, Part D, Protista 3 (Protozoa, Chiefly Radiolaria and Tintinnina)*, ed Moore RC (The Geological Society of America & The University of Kansas, Boulder & Lawrence), pp 1–195.
9. Okulitch V (1995) *Treatise on Invertebrate Paleontology, Part E, Archaeocyatha and Porifera*, ed Moore RC (The Geological Society of America & The University of Kansas, Boulder & Lawrence), pp 1–122.
10. Hill D (1972) *Treatise on Invertebrate Paleontology, Part E, Archaeocyatha*, ed Teichert C (The Geological Society of America & The University of Kansas, Boulder & Lawrence), *Vol. 1, second edition*, pp 1–158.
11. Finks RM, Reid REH, Rigby JK (2003) *Treatise on Invertebrate Paleontology, Part E, Porifera*, ed Kaesler RL (The Geological Society of America & The University of Kansas, Boulder & Lawrence), *Vol 2, revised*, pp 1–349.
12. Finks RM, Reid REH, Rigby JK (2004) *Treatise on Invertebrate Paleontology, Part E, Porifera*, ed Kaesler RL (The Geological Society of America & The University of Kansas, Boulder & Lawrence), *Vol. 3, revised*, pp 1–872.

13. Bayer F, *et al.* (1956) *Treatise on Invertebrate Paleontology, Part F, Coelenterata*, ed Moore RC (The Geological Society of America & The University of Kansas, Boulder & Lawrence), pp 1–358.
14. Hill D (1981) *Treatise on Invertebrate Paleontology, Part F, Coelenterata, Supplement 1 (Rugosa and Tabulata)*, ed Teichert C (The Geological Society of America & The University of Kansas, Boulder & Lawrence), pp 1–762.
15. Brasier M, Green O, Shields G (1997) Ediacarian sponge spicule clusters from southwestern Mongolia and the origins of the Cambrian fauna. *Geology* 25:303–306.
16. Kremer JR, Mastronarde DN, McIntosh JR (1996) Computer visualization of three-dimensional image data using IMOD. *J Struct Biol* 116:71–76.
17. Vali H, Forster O, Amarantidis G, Petersen N (1987) Magnetotactic bacteria and their magnetofossils in sediments. *Earth Planet Sci Lett* 86:389–400.
18. Zachos JC, *et al.* (2006) Extreme warming of mid-latitude coastal ocean during the Paleocene-Eocene Thermal Maximum: Inferences from TEX86 and isotope data. *Geology* 34:737–740.
19. Coplen TB, Kendall C, Hopple J (1983) Comparison of stable isotope reference samples. *Nature* 302:236–238.

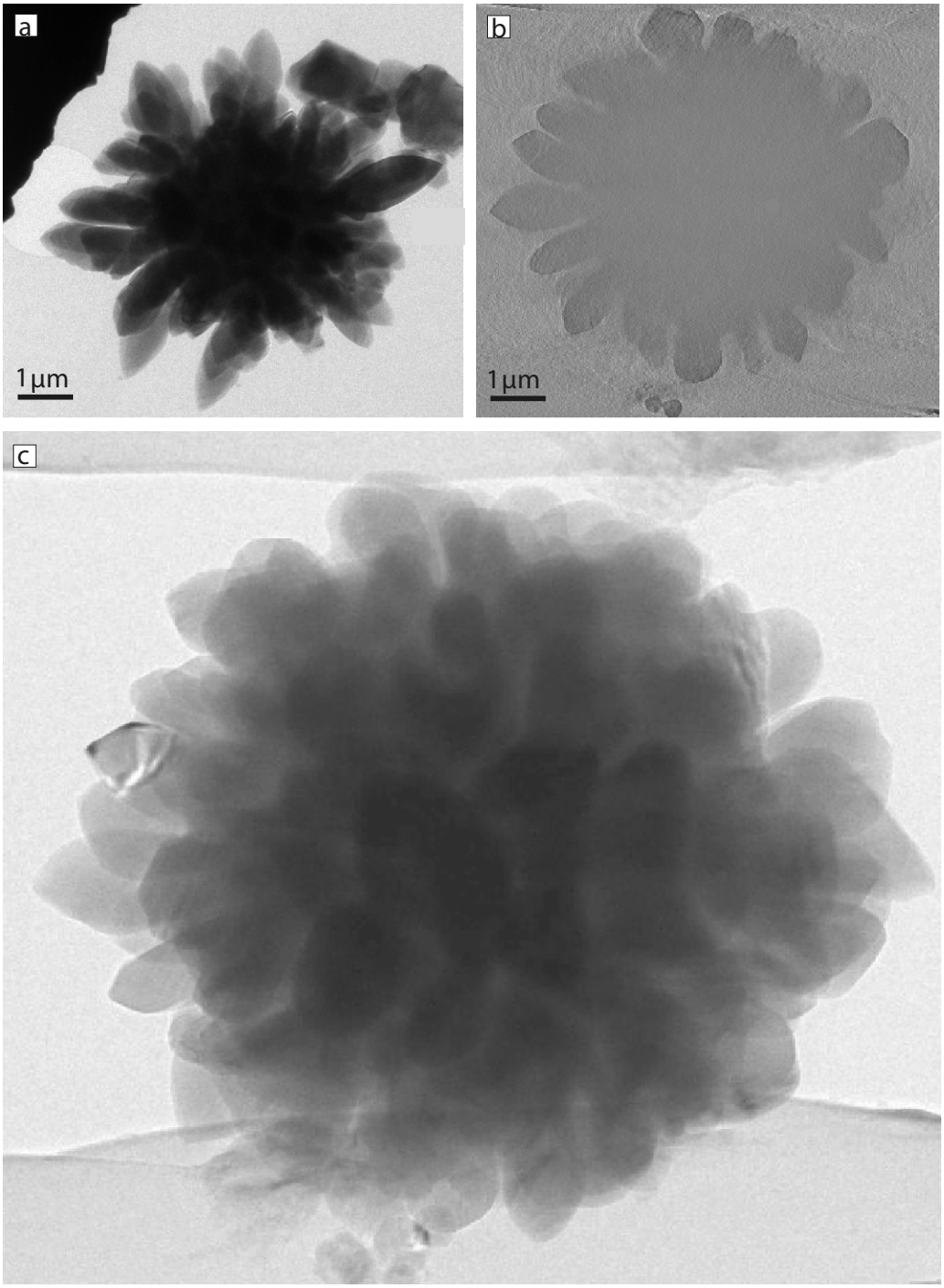

Fig. S1. (*a*) Conventional TEM image of spearhead-like magnetite particles arranged into a radial, flower-like structure. All particles are aligned with their stalk oriented toward the center of the structure. (*b*) Cross section of a 3D reconstructed tomography image shows that the central region of the radial, flower-like structure appears opaque and may also be iron-enriched. The tomogram was calculated from a tilt series of images (Movie S1) of the radial, flower-like structure using IMOD (16). (*c*) Still image of the tomogram (Movie S1).

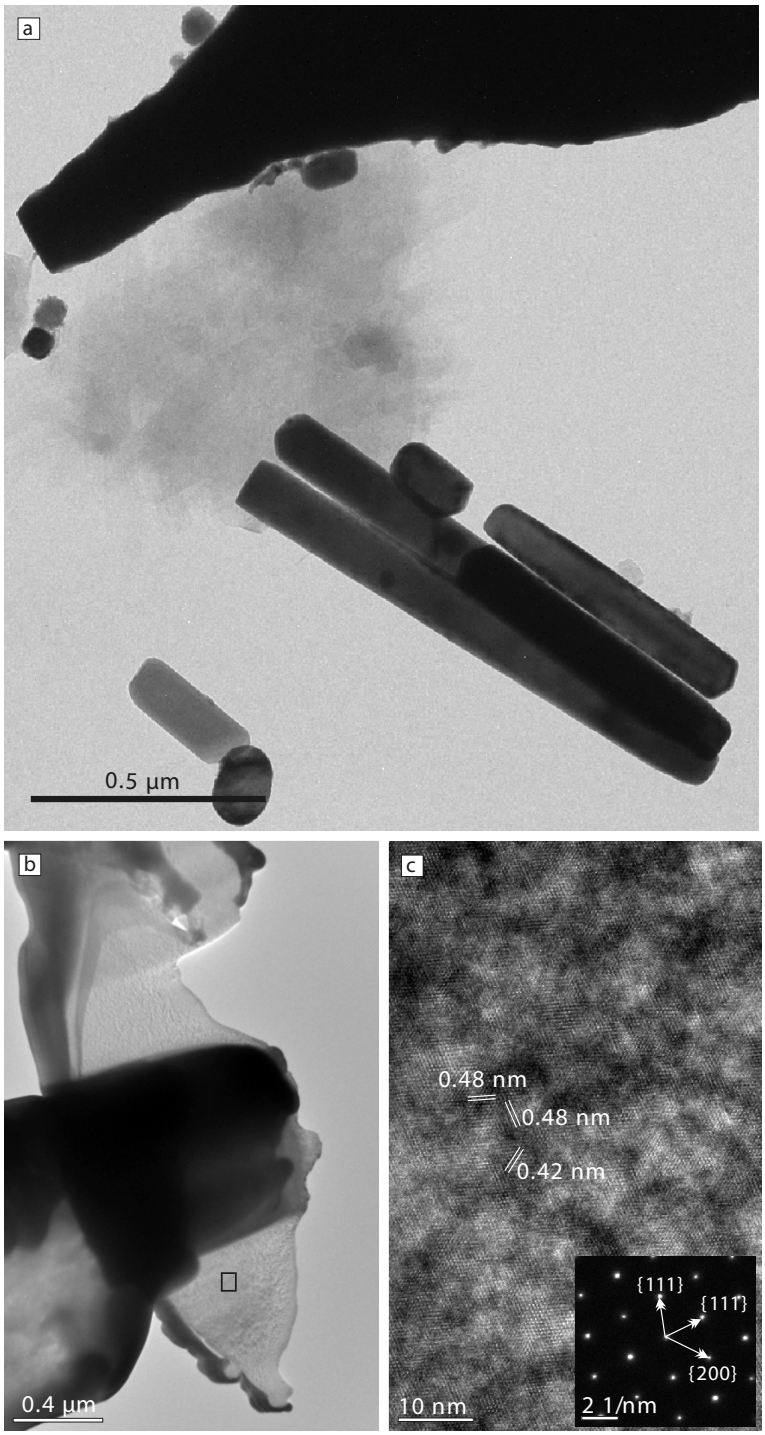

Fig. S2. TEM images of elongated prismatic and spearhead-like magnetite particles. (*a*) A cluster of elongated prismatic magnetite particles (center) and a part of a spearhead-like magnetite particle (upper part of the image) along with scattered bacterial magnetite. (*b*) TEM image shows a focused ion beam (FIB) milled ultrathin section of a spearhead-like magnetite particle that was thinned from both sides to a thickness of 100 nm parallel to the long axis and mounted to the grid with tungsten (black area in the center). (*c*) Two sets of lattice fringes with a *d*-spacing of 0.48 nm {111} and one with 0.42 nm {200}, respectively. The {111} and {200} diffraction planes are indicated by arrows in the *Inset* of *c*. The location of *c* is marked by the box in *b*.

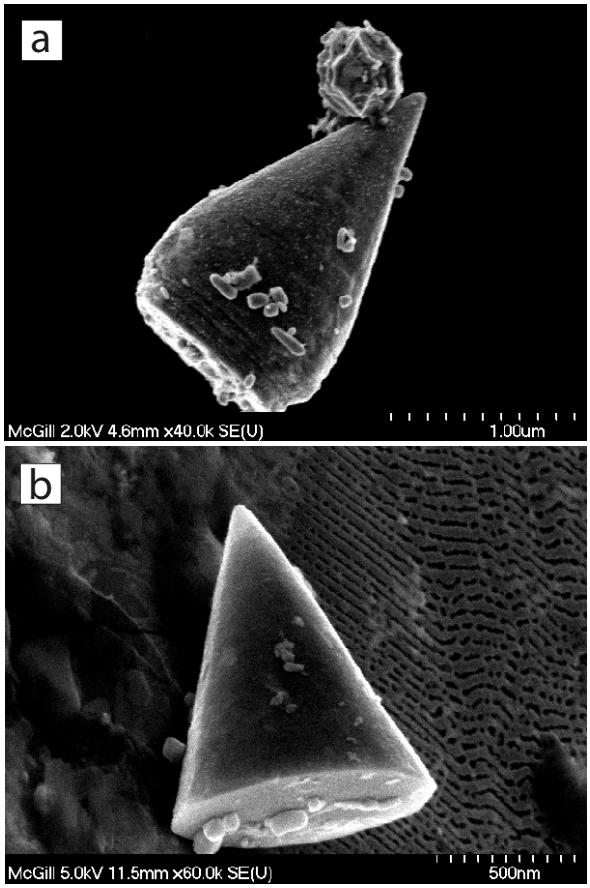

Fig. S3. SEM images of parting in spearhead-like particles along {220} planes. The parting perpendicular to the long axis of the spearhead-like particle occurs at different locations and suggests that the lower part of these particles, including the stalk, is composed of disk-like subunits. Because the whole particle shows single crystal structure and no lattice disruption is observed at the parting (see Fig. S2*c*), epitactic-like growth may be responsible for the disk-like morphology. Parting might be produced by shear stress imposed upon the crystals, either *in vivo*, attesting to a hypothesized protective biological function and/or cytoskeletal fastening of the stalk ends in contrast with extracellular free spearhead-like tips, or by diagenetic compaction.

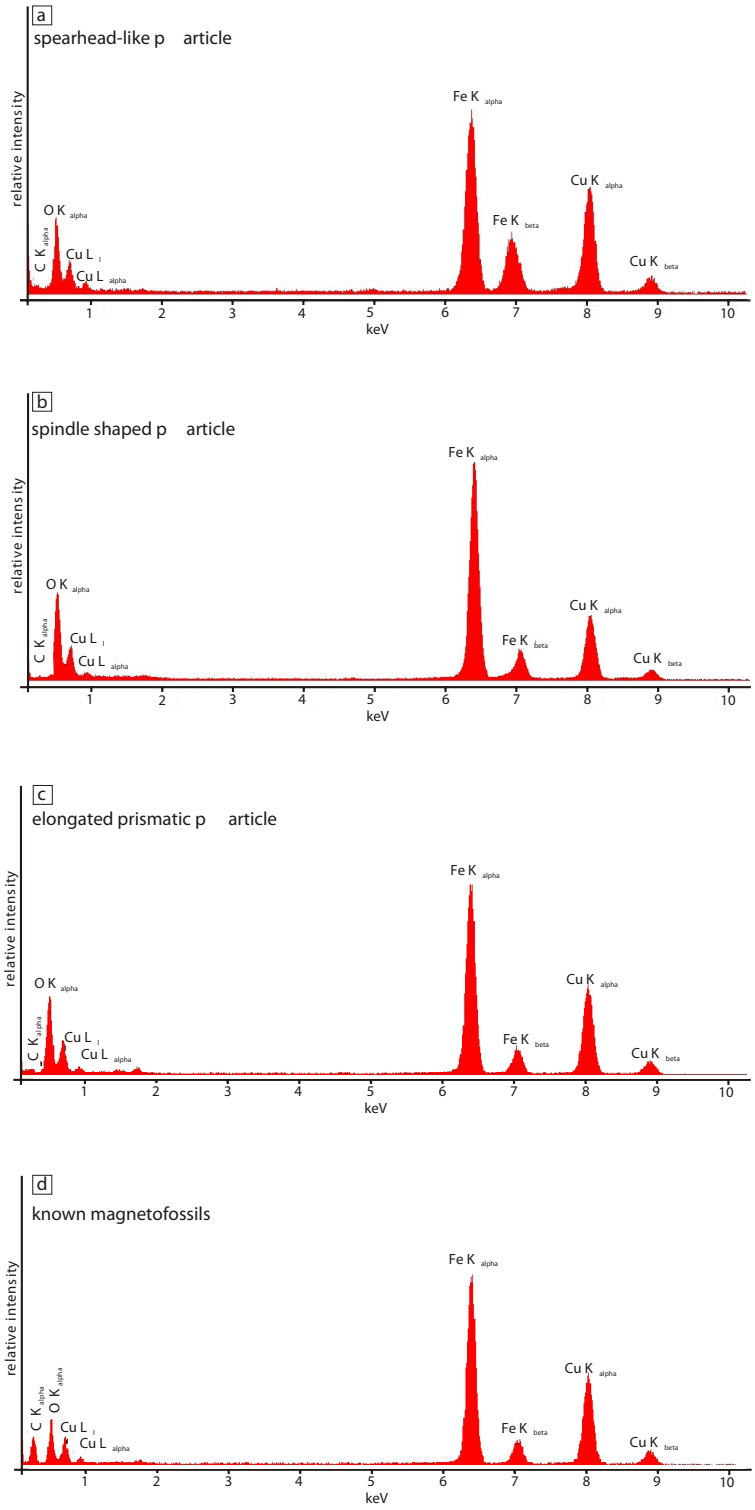

Fig. S4. Energy dispersive x-ray spectroscopy analysis of a spearhead-like particle (*a*), a spindle-shaped particle (*b*), an elongated hexaoctahedral particle (*c*), and a known bacterial magnetofossil (*d*). The analyses show that the novel crystals (*a–c*) are composed of iron and oxygen, which is consistent with the composition of bacterial magnetofossils (*d*). No other impurities are associated with these particles. The Cu and C peaks in the spectra are from the TEM grid. The EDS analysis does not provide any stochiometric information on the oxidation state of the Fe in these particles. It most likely, however, that these particles are oxidized to maghemite as shown in magnetofossils from marine environments (17).

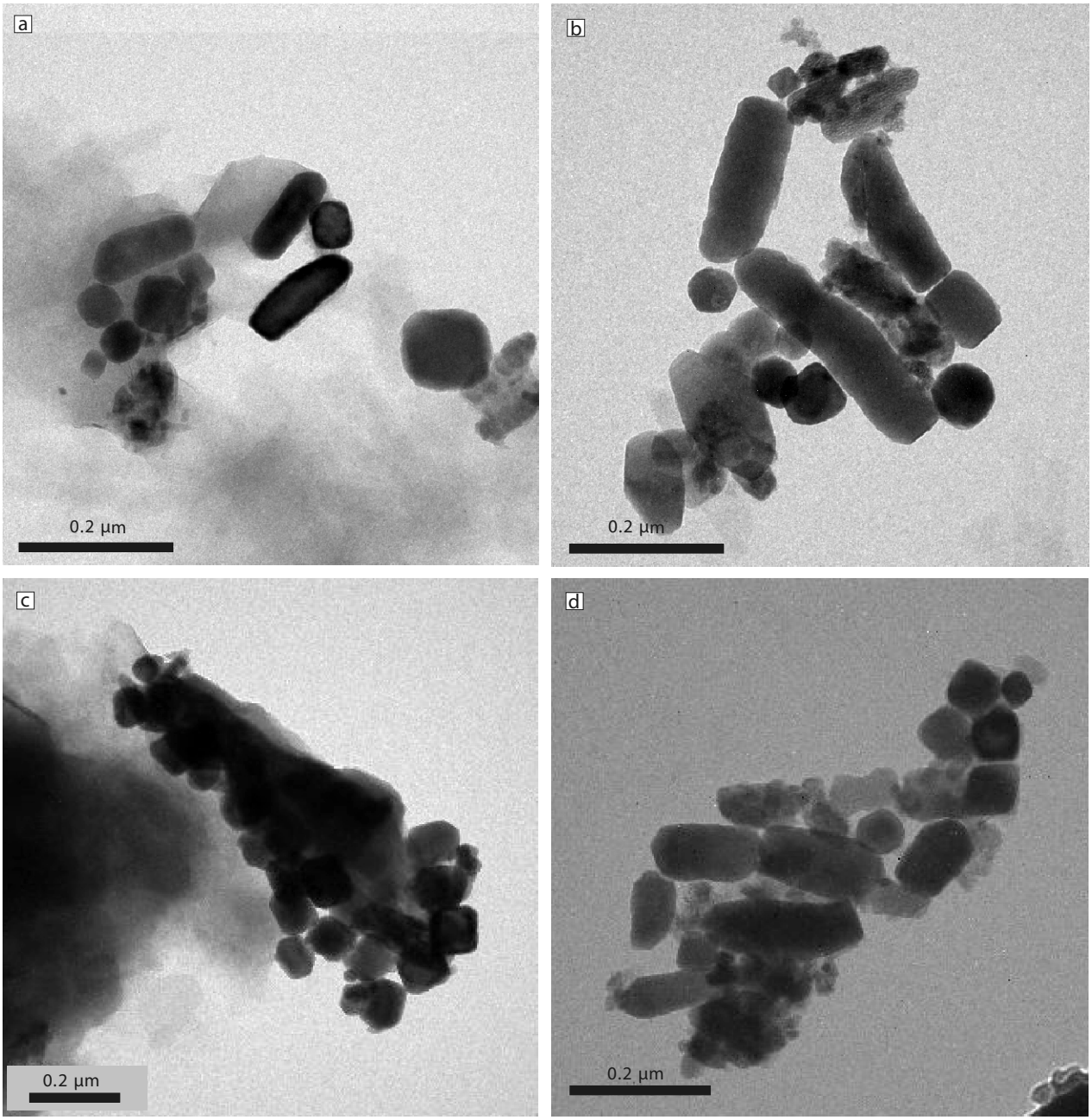

Fig. S5. TEM images of bacterial magnetofossils extracted from sediments above (165.81 m) (*a* and *b*) and below (173.15 m) (*c* and *d*) the PETM clay. They show different size and shape of well preserved bacterial magnetofossils, including prismatic, bullet-shaped, and diamond-shaped.

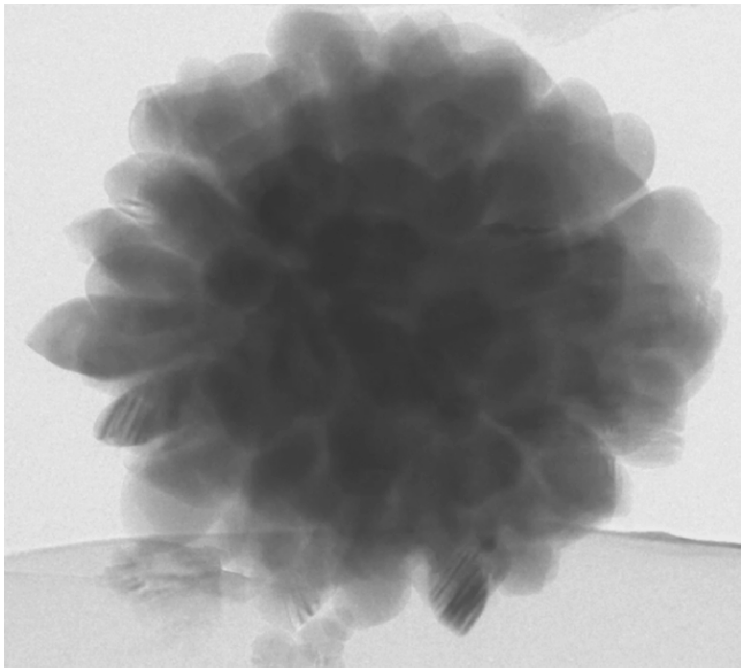

Movie S1. Using a FEI Titan 300-kV FE-STEM equipped with a Gatan Ultrascan 1000 4k × 4k CCD camera, a movie was constructed from a complete tilt series of images recorded every 2° from −70° to 66° of a radially arranged, spearhead-like magnetite particle. Images were aligned by using IMOD (16) after selecting 16 features as fudicial markers.

Movie S1 (MOV)

Table S1. Paleotemperature calculations

$\bar{x}$ ($^{18}O/^{16}O$)	SE $\bar{x}$		$\delta^{18}O_{Spear}$ (VSMOW)	$\delta^{18}O_{Cib}$ (VPDB)	$\delta^{18}O_{Cib}$ (VSMOW)	$\alpha_{(Cc\text{-}Mt)}$	$10^3 \times \ln \alpha_{(Cc\text{-}Mt)}$	Temperature, K	Temperature, °C
2.002859	0.006463	Minimum	−4.390	−3	27.817	1.032	31.837	268.58	−4.57
		Mean	−1.167	−3	27.817	1.029	28.605	285.84	12.69
		Maximum	2.056	−3	27.817	1.026	25.384	306.86	33.71

Calcite–magnetite fractionation equation: $10^3 \times \ln\alpha_{(Cc\text{-}Mt)} = 1.99 \times (10^6/T^2) + 4.25$. $\bar{x}$, weighted mean of $^{18}O/^{16}O$ of the spearhead-like magnetite particle; SE $\bar{x}$, standard error of the weighted mean; Spear, spearhead particle; Mt, magnetite; Cc, calcite; *Cib*, *Cibicidoides*; VSMOW, Vienna standard mean ocean water; VPDB, Vienna PeeDee belemnite. Values for *Cibicidoides* are from ref. 18; conversion of $\delta^{18}O_{VPDB}$(*Cibicidoides*) to $\delta^{18}O_{VSMOW}$(*Cibicidoides*) is from ref. 19.